Tunable refraction and reflection of self-confined light beams

MARCO PECCIANTI[1]*, ANDRIY DYADYUSHA[2], MALGOSIA KACZMAREK[2] AND GAETANO ASSANTO[1]*

[1]NooEL—Nonlinear optics and optoElectronics Lab, Department of Electronic Engineering, INFN and CNISM, University "Roma Tre", Via della Vasca Navale 84-00146, Rome, Italy
[2]School of Physics and Astronomy, University of Southampton, Southampton SO17 1BJ, UK
*e-mail: m.peccianti@uniroma3.it; assanto@uniroma3.it

Light filaments or optical spatial solitons are self-confined (non-spreading) beams that originate from the balance between diffraction and self-focusing in nonlinear optical media (those with a response dependent on the level of excitation)[1–3]. Owing to their ability to self-trap as well as to guide weaker signals (even if differing in colour or modulation format) within the waveguides or 'light-pipes' they induce, optical spatial solitons could form the basis of future all-optical processing networks[4,5]. One of the most interesting challenges in soliton propagation and engineering concerns light filaments incident on linear/nonlinear or nonlinear/nonlinear interfaces. Here we report the robust propagation, refraction and reflection of optical spatial solitons at the interface between two regions of a nematic liquid crystal. The ability to independently tune the optical properties of each region enables us to steer the beams by refraction and total internal reflection by as much as -18 and $+22$ degrees, respectively. Moreover, the extended (nonlocal) and anisotropic response of our system supports polarization healing of the solitons across the interface as well as non-specular filament reflection. Finally, exploiting the inherent and all-optically tunable birefringence, we demonstrate unprecedented nonlinear Goos–Hänchen lateral shifts in excess of 0.5 mm.

Optical spatial solitons have been investigated in a variety of nonlinear materials, both in one- and two-dimensional geometries[1–3]. In a few cases, the problem of filaments reaching an interface has been tackled theoretically with reference to cubic[6–10] and quadratic responses[11], and experimental demonstrations have been reported in quadratically nonlinear media at grazing incidence[12,13], in cubically nonlinear semiconductor waveguides with a prism electrode[14] and in prism-shaped photovoltaic crystals[15]. The manner in which molecules reorient and arrange themselves in a nematic liquid crystal (NLC) gives rise to both a strong electro-optic response and a giant non-resonant optical nonlinearity[16,17]. The latter of these properties, in conjunction with the non-local nature of molecular ordering in NLCs, enables them to support stable, low-power two-dimensional solitons[18–21], whereas the former allows distinct regions of a liquid crystalline structure to be independently tuned by the application of different voltages. This entails the definition of voltage-adjustable transitions between birefringent uniaxial media differing in refractive index,

orientation and nonlinear response, which in turn offers a great deal of versatility in the study of light propagation and localization phenomena at and across interfaces.

NLCs consist of elongated rod-like molecules with refractive indices $n_\parallel$ and $n_\perp$ along and orthogonal to their main axis (or director $\mathbf{n}$), respectively. Several liquid crystals in the nematic phase[16] are positive uniaxial materials ($n_\parallel > n_\perp$) and can exhibit a large birefringence and a giant molecular nonlinearity. An incident extraordinarily polarized optical beam, with electric field non-orthogonal to $\mathbf{n}$, can interact with the induced dipoles and force the molecular reorientation. Such reorientational response enabled us to observe anisotropic spatial solitons in planar cells, the so-called nematicons[18], as well as their interaction, periodic breathing, transverse dynamics and walk-off[20–22]. As reorientation can also be driven by a low-frequency electric field, for example, through a voltage applied across the thickness of the NLC cell[16,17], linear, nonlinear and nonlocal properties of the medium can be externally adjusted[23]. As a result, the system is very adaptive, tunable and amenable to the exploration of various geometries, for example, defining specific regions and interfaces via tailored electrodes.

We examine a cell consisting of two parallel glass slides that confine a thick layer of NLCs. As shown in Fig. 1a, we take z as the direction normal to the cell input facet and x as the direction normal to the electrodes (that is, across the NLC thickness). Anchoring films at the cell boundaries and a voltage applied via transparent electrodes determine the director alignment in the bulk of the medium. As the top electrode is split in two, a different potential can be applied to each part with respect to the bottom ground plane (see Fig. 1a). These two regions of the liquid crystal cell are labelled as 1 and 2 and are ideally separated by the plane xp, with p being a straight line bisecting the 'gap' (of finite width G) at an angle Θ with respect to z in the plane yz. We consider the structure invariant along p and define a rotated framework xtp (see Fig. 1b) with $t \perp p$. The director $\mathbf{n}$ is at an angle ξ above the plane tp and its azimuthal angle is ρ with respect to t, that is, $\mathbf{n}(x, t, p) \equiv \mathbf{n}(\sin \xi, \cos \xi \cos \rho, \cos \xi \sin \rho)$. The reorientation induced by an externally applied low-frequency electric field $\mathbf{E} = (E_x, E_t, 0)$ is governed by the Poisson equation

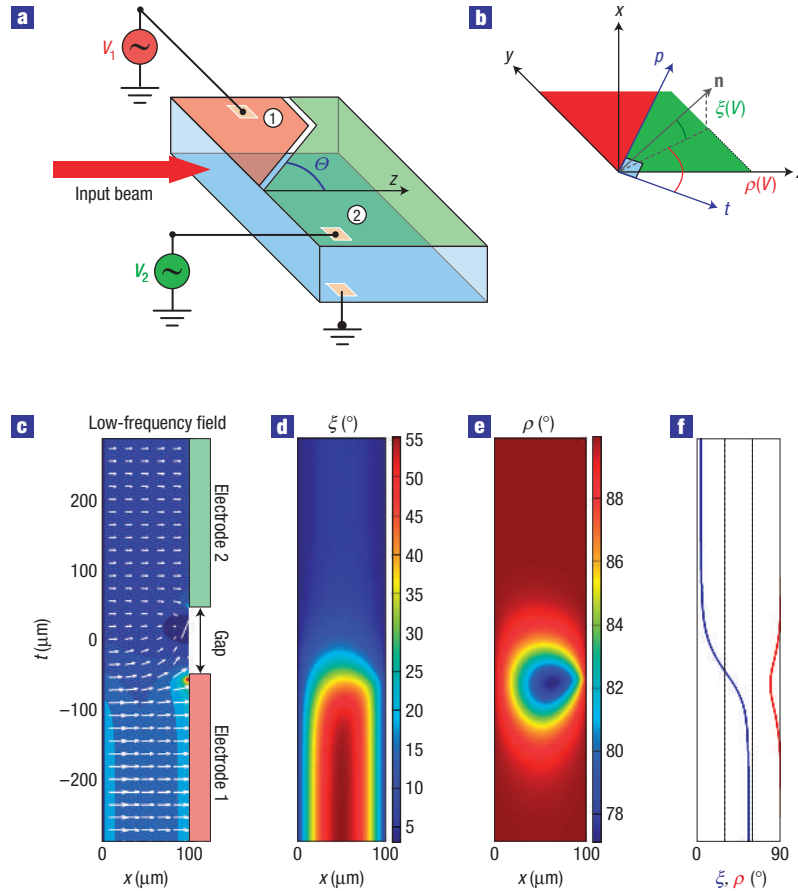$$\nabla \cdot (\bar{\bar{\varepsilon}} \mathbf{E}) = 0$$

Figure 1 The sample and its electro-optic response. a, Schematic diagram of the liquid crystalline cell with two regions. On the top side, two electrodes are separated by a straight gap of width G at an angle Θ with z. **b**, Unequal voltages V_1 and V_2 applied to regions 1 and 2, respectively, induce different reorientations ξ and ρ of the director **n**. As a result, these regions exhibit different extraordinary refractive indices n_{e1} and n_{e2}, respectively. p and t are parallel and orthogonal to the gap line separating the electrodes, respectively. **c–f**, Calculated electrostatic and reorientational effects from equation (1) for $V_1 = 1.5\,\mathrm{V}$ and $V_2 = 0.7\,\mathrm{V}$: low-frequency electric-field distribution in the plane xt (red is more intense) (**c**); reorientation ξ (**d**) and ρ (in degrees) versus x (**e**) and in the cell mid-plane ($x = 50\,\mu\mathrm{m}$) (**f**), respectively, for $\xi_0 = 0.017\pi$ and $\rho_0 = 0.5\pi$ at $V_1 = V_2 = 0\,\mathrm{V}$. Material parameters refer to liquid crystal E7 (see the Methods section).

with the elements of the dielectric tensor depending on the director projection onto the reference axes, that is, $\varepsilon_{ij} = \varepsilon_\perp \delta_{ij} + \varepsilon_a n_i n_j$ with $i, j \in (x, t, p)$. Using a standard variational approach applied to the interaction energy between field and director (see Supplementary Information, Section S1), we derive:

$$
\begin{cases}
2\varepsilon_a E_x E_t \cos 2\xi \cos \rho + \varepsilon_a \sin 2\xi \left(E_x^2 - E_t^2 \cos^2 \rho \right) \\
\quad + K \sin 2\xi \left[\left(\dfrac{\partial \rho}{\partial x} \right)^2 + \left(\dfrac{\partial \rho}{\partial t} \right)^2 \right] + 2K\nabla^2 \xi = 0 \\[2ex]
\varepsilon_a E_x E_t \sin 2\xi \sin \rho + \cos \xi \left[\varepsilon_a E_t^2 \cos \xi \sin 2\rho \right. \\
\quad \left. + 4K \sin \xi \left(\dfrac{\partial \xi}{\partial x} \dfrac{\partial \rho}{\partial x} + \dfrac{\partial \xi}{\partial t} \dfrac{\partial \rho}{\partial t} \right) - 2K\nabla^2 \rho \right] = 0
\end{cases}
\tag{1}
$$

K is a scalar elastic coefficient for splay, bend and twist of the NLC molecules[16]. Equation (1) can be integrated with boundary conditions $\rho(x = 0) = \rho(x = L) = \rho(V = 0) = \rho_0$ and $\xi(x = 0) = \xi(x = L) = \xi(V = 0) = \xi_0$ stemming from the anchoring at the interfaces, with L being the cell thickness.

Figure 1c shows the calculated molecular reorientation for a cell with $L = 100\,\mu\mathrm{m}$ and pretilt $\xi_0 = 0.017\pi$, with the liquid crystal director initially parallel to p (that is, $\rho_0 = 0.5\pi$) and

the electrode gap $G = 100\,\mu\mathrm{m}$. For low-frequency ($f_{\mathrm{bias}} = 1\,\mathrm{kHz}$) voltages $V_1 = 1.5\,\mathrm{V}$ and $V_2 = 0.7\,\mathrm{V}$ in phase at the electrodes, a maximum reorientation $\xi(x = L/2) = 0.3\pi$ is obtained in region 1, whereas the field in region 2 is below the reorientational (Freedericks) threshold[17]. This results in an index change for extraordinarily polarized beams propagating across p.

Owing to the significant NLC optical birefringence, a plane wave incident at the interface between regions 1 and 2 and extraordinarily (e) polarized (its electric field in the principal plane **nk** defined by the optical axis and the unit wavevector $\mathbf{k}/|\mathbf{k}|$) is expected to undergo refraction when $V_2 > V_1$ (that is, refractive index n_{e1} smaller than refractive index n_{e2} for the same optical unit wavevector $\mathbf{k}/|\mathbf{k}|$ in regions 1 and 2, respectively) and total internal reflection (TIR) when $V_1 > V_2$ ($n_{e1} > n_{e2}$) for incidence angles larger than a critical value. The behaviour of a light filament encountering such an interface is truly intriguing as, to maintain its self-confinement by nonlinear reorientation, it must remain e-polarized on either refraction or reflection[21].

We excited a nematicon by launching a 4.5 mW gaussian beam ($\lambda = 1{,}064\,\mathrm{nm}$) into the NLC cell ($\rho_0 = 0.5\pi$ and $\xi_0 = 0.017\pi$) with input wavevector $\mathbf{k}$ at an angle $\Phi_1 = 0.44\pi$ (79°) with t. Figure 2 shows images of the filament propagation in the plane yz
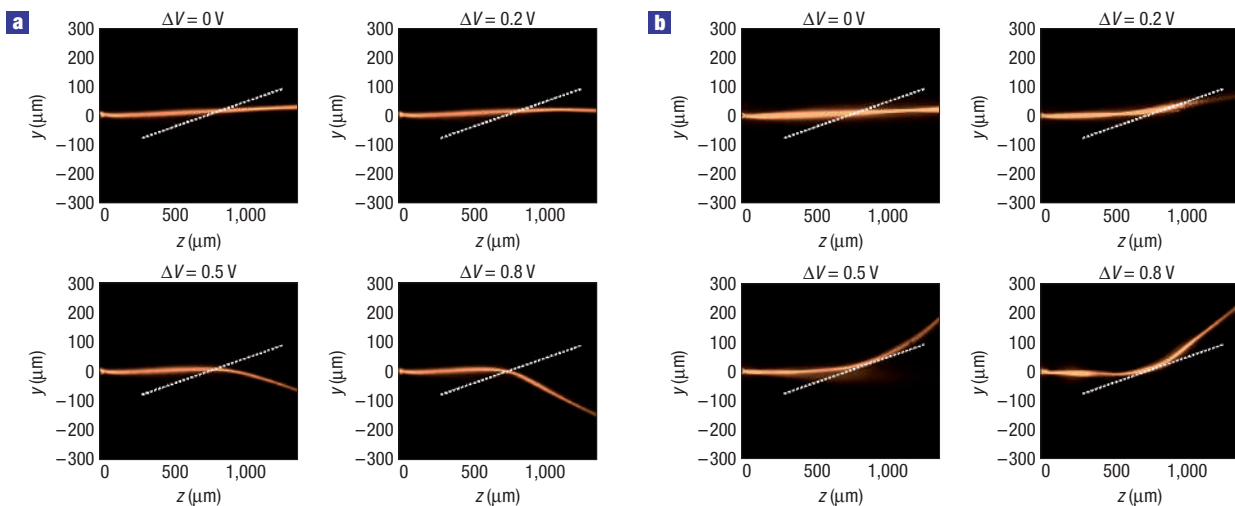
Figure 2 Intensity evolution of a 4.5 mW (input power) nematicon launched at $\Phi_I = 0.44\pi$ with respect to t in a sample with $\rho_0 = 0.5\pi$ and $\xi_0 = 0.017\pi$. **a**, For $\Delta V = V_1 - V_2 \le 0$ V, the filament is refracted at the interface between regions 1 and 2. **b**, By making region 1 optically denser than region 2 ($\Delta V \ge 0$ V), the nematicon can undergo TIR for $\Delta V > 0.5$ V, as demonstrated in the bottom panels. For $\Delta V = 0.2$ V (**b**, upper right panel) the beam loses self-confinement and diffracts because nonlinearity in region 2 is minimized as the wavevector **k** approaches the director alignment **n** (that is, the e-wave turns into an ordinary ray).

for $V_2 > V_1$ (Fig. 2a) and $V_1 > V_2$ (Fig. 2b), respectively. Keeping $V_1 = 0.7$ V and increasing V_2 from 0.7 to 1.5 V, strong filament refraction occurred. The amount of refraction could be adjusted by varying $\Delta V = V_1 - V_2$ from 0 to -0.8 V across the gap G. Conversely, for $V_2 = 0.7$ V and $\Delta V \ge 0.5$ V, we observed TIR of the self-confined beam (Fig. 2b). The latter is the first demonstration of TIR of a soliton waveguide at a nonlinear/nonlinear interface in cubically nonlinear media. Noticeably, the system could be continuously tuned from straight-on propagation to refraction or to reflection by simply varying ΔV. One striking feature of the nonlinear propagation of such a self-trapped filament through an interface is that its electric field remains e-polarized after refraction. In fact, the nematicon rotates its (extraordinary) electric-field vector to keep it in the principal plane **nk**, as the optical axis **n** adiabatically turns in the gap separating region 1 from 2 (see Supplementary Information, Section S2). Furthermore, even after TIR ($V_1 > V_2$) the propagation of an ordinarily polarized field component is forbidden owing to momentum (wavevector) conservation along p (see Supplementary Information, Section S2). Hence, through polarization healing, all the power (ideally) remains bound with the e-wave soliton (Fig. 2b).

For the case of refraction ($\Delta V < 0$), acquired and recorded trajectories of light filaments are shown in Fig. 3a. The non-diffracting beam is angularly steered by as much as 18° by increasing the V_2 voltage, which corresponds to a lateral shift $\Delta y \approx -210$ μm after propagating for 1.4 mm. The latter is equivalent to more than 20 Rayleigh lengths of the linear beam.

Figure 3b presents the filament trajectories for the case of TIR, which occurs for $\Delta V > 0$. For $\Delta V = 0.8$ V, mirror-like reflection is observed and the filament is deviated by as much as 22°, corresponding to a measured lateral shift $\Delta y \approx 200$ μm after a propagation distance of 1.4 mm. For $V_1 > 1.5$ V, the filaments were affected by significant transverse (x) dynamics, preventing them from propagating in the cell mid-plane through the gap (see Supplementary Information, Section S3). Whereas the measurements can only reveal the angular steering of the Poynting vector **S** (the energy flux) across the interface 1–2, the walk-off angle δ between **S** and the wavevector **k** depends on the

angle θ between **k** and **n** (with **S** lying in the plane **nk** between **n** and **k** if $n_\parallel > n_\perp$)[21]. Therefore, with reference to the interface along p, the incidence angle Φ_{IS} (with respect to t) of **S** differs from the incidence angle Φ_I of the wavevector **k** by the apparent walk-off δ_{yz} (ref. 21), that is, the walk-off angle as visible in the observation plane yz (see Fig. 4). As an out-of-plane component of **S** corresponds to a filament up- or down-shift along x, such additional transverse dynamics affects the soliton x position across the interface and limits the bias mismatch $|\Delta V|$ to be used to observe TIR.

Refraction and reflection of a self-confined nematicon filament at a graded-index anisotropic interface between voltage-tunable nonlinear media encompass some remarkable physics. In the presence of optical anisotropy, the direction of transmitted and reflected rays depends on the orientation of the optical axis (see Supplementary Information, Section S2). In the geometry illustrated above ($\rho_0 = 0.5\pi$), the angles (Φ_{IS}, Φ_{TS}, Φ_{RS}) formed by the Poynting vectors of incident, transmitted and reflected filaments, respectively, are always larger than those (Φ_I, Φ_T, Φ_R) of the corresponding wavevectors; as the director is aligned with p, for the reflected filament $\Phi_R = \Phi_I$ and, therefore, $\Phi_{RS} = \Phi_{IS}$. It is worth noting, however, that for $\rho_0 \ne 0.5\pi$ the walk-off of a nematicon can cause non-specular ($\Phi_R \ne \Phi_I$) TIR, that is, the beam reflected at the interface (and eventually exiting a cell with parallel input and output facets) would not be the mirror-like reflection of the incident one. To this extent, let us consider the propagation of a filament in a cell with, for example, $\rho_0 = 0.28\pi$ and potentials $V_1 = 1.5$ V and $V_2 = 0$ V, respectively, as shown in Fig. 4. An e-wave filament is totally reflected with incidence and emergence angles $\Phi_{IS} = 79.0°$ and $\Phi_{RS} = 79.5°$, respectively. In such a case, $\Phi_I = \Phi_{IS} + \delta_{yz\_I}$, whereas $\Phi_R = \Phi_{RS} - \delta_{yz\_R}$, with δ_{yz_I} and δ_{yz_R} being the apparent walk-off angles associated with the incident and reflected beams, respectively. For nematicons propagating (at moderate ΔV) along the middle of the cell (the 'mid-plane' $x = L/2$), we estimated δ_{yz_I} and δ_{yz_R} and, correspondingly, $\Phi_I = 81.1°$ and $\Phi_R = 76.6°$, a net asymmetric reflection. However, as in general $\delta_{yz\_j}(x, y, z) \ge \delta_{yz\_j}(L/2, y, z)$ along the whole trajectory due to filament transverse dynamics
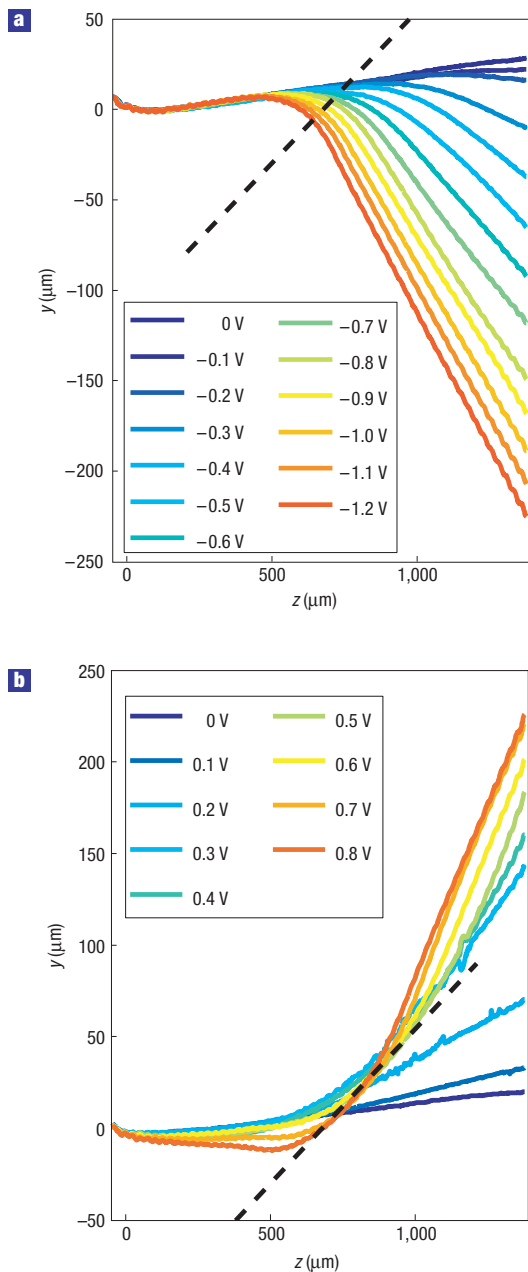
Figure 4 Asymmetric TIR in the presence of optical anisotropy. a, Photograph of a nematicon undergoing TIR for $V_1 = 1.5$ V and $V_2 = 0$ V. **b,** The Poynting vectors $\mathbf{S}_{in}$ and $\mathbf{S}_{out}$ of incident and reflected filaments differ in angle from their corresponding wavevectors $\mathbf{k}_I$ and $\mathbf{k}_R$ by the apparent walk-offs $\delta_{yz,I}$ and $\delta_{yz,R}$, respectively.

linear indices depends on excitation[7,8], in our case the effective nonlinearity is higher in region 2 (ref. 23), hence filament-driven reorientation tends to reduce the index mismatch. Assuming the medium stratified along t with extraordinary index constant in each layer $t = t_j$, the filament trajectory bends[24] with an emerging (reflected) beam being displaced more and more along p as the input power increases. This nonlinear Goos–Hänchen shift[25], typically limited to small values even at large (grazing) incidence angles, can be addressed experimentally with $(2 + 1)$ D spatial solitons in our non-local voltage-tunable NLC sample (see Supplementary Information, Section S4). Figure 5 shows filament trajectories and nonlinear Goos–Hänchen shift in the sample of Fig. 4 ($\rho_0 = 0.28\pi$), for $\Phi_{IS} = 79.5°$ and increasing optical excitations.

Our study of light filaments and their self-induced waveguides in nonlocal and nonlinear media revealed some very unique properties. First, light filaments can propagate across an interface, not only surviving changes in linear refractive properties, but also maintaining their self-confined character as nonlinearity and anisotropy vary. Second, by demonstrating such phenomena in NLCs and across a voltage-defined boundary, we achieved an unprecedented soliton steering from -18 to $22°$ using moderate voltages and milliwatt optical powers. Furthermore, by making the material optical anisotropy work to our advantage, we verified that optical filaments not only maintain the extraordinary polarization required for self-guiding, but they also experience voltage-adjustable as well as nonlinear Goos–Hänchen shift and non-specular reflection. Such findings bridge some of the gaps between various soliton-related phenomena of nonlinear physics in anisotropic media and unveil rich scenarios for the implementation of soliton-based optical circuits and reconfigurable photonic interconnects.

METHODS

Here we present some details on sample preparation and experiments. Supplementary Information, Section S1 contains details on the model and its derivation.

Figure 3 Filament trajectories in the plane yz versus voltage difference ΔV between regions 1 and 2. a, Refraction of a nematicon. **b,** TIR of a nematicon. The dashed line represents the interface between regions 1 and 2. The initial trajectories near $z = 0$ are affected by the director distortion at the cell input (see the Methods section).

across the thickness of the cell (out of the mid-plane), the actual difference $\Phi_I - \Phi_R$ is generally larger than in our evaluation (see Supplementary Information, Section S2). Note that a small angular contribution to the angle of the reflected filament is due to the nonlinear response associated with filament propagation. The latter contribution, however, is much smaller than the anisotropic effect and below our experimental accuracy.

TIR is normally defined by the linear index mismatch between two media. Although it is understood that TIR of finite-size beams at the boundary between two nonlinear materials of different
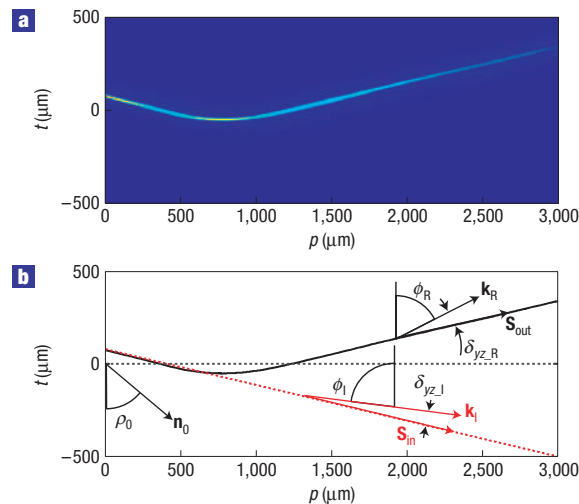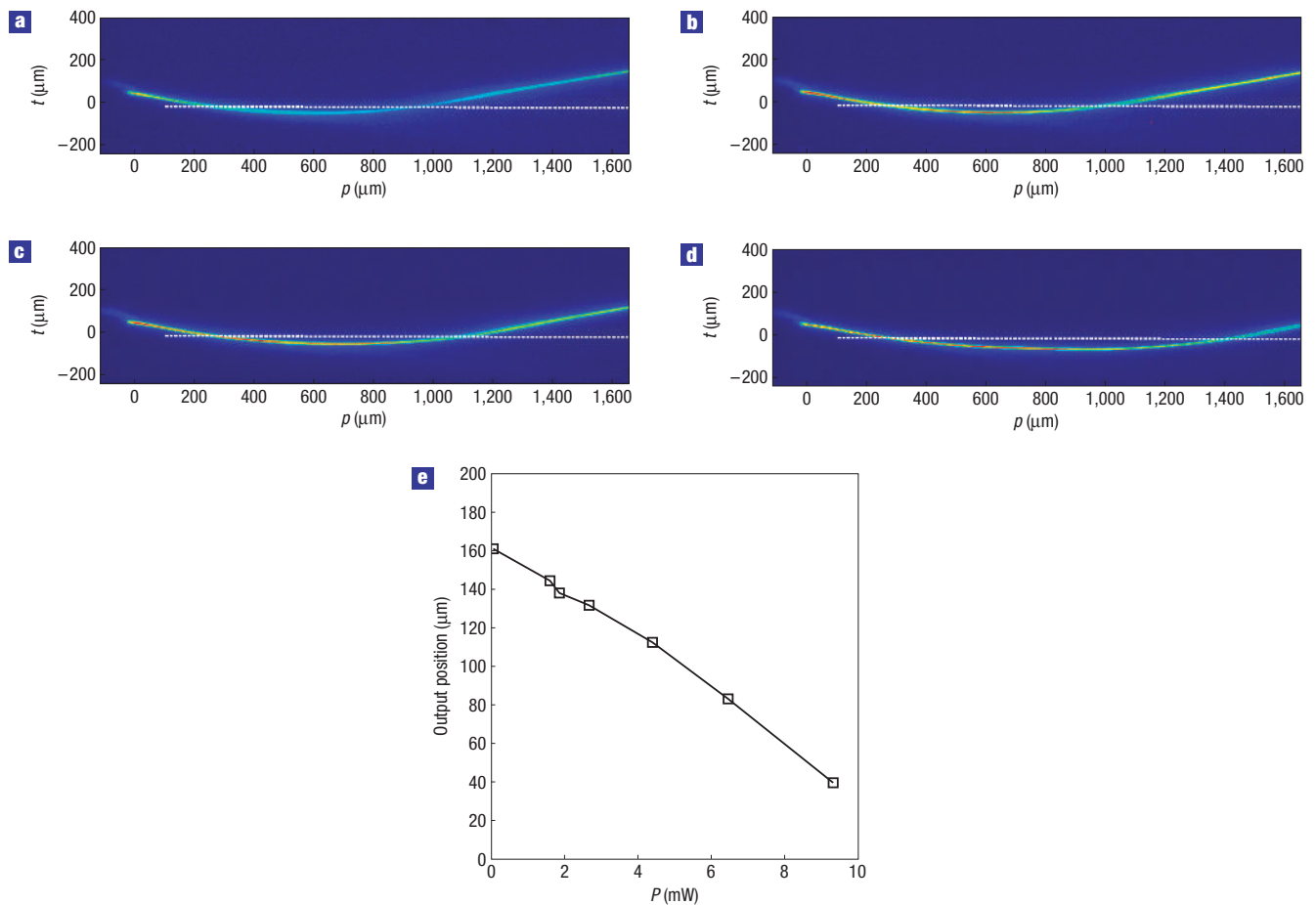
Figure 5 Nonlinear Goos–Hänchen shift under TIR. a–d, Photographs of filament trajectories for various optical excitations (input powers), namely $P = 1.60$ (**a**), 2.67 (**b**), 4.40 (**c**) and 9.33 mW (**d**). The displacement of the reflected filament along p increases with power. The horizontal dashed line corresponds to the gap line p. **e,** Filament position along t at $p = 1.6$ mm for input powers ranging from 0.05 (linear limit) to 9.33 mW.

SAMPLES

For our experimental study, we constructed cells consisting of two glass slides coated with transparent indium tin oxide (ITO) electrodes for the application of low-frequency voltage biases, with an NLC inbetween (see Fig. 1a). Separate electrodes defining regions 1 and 2 were created on one glass substrate through standard lithography and chemical etching. On the second substrate (parallel to the first one, that is, in the plane xy), see Fig. 1, the original ITO electrode was kept uniform to serve as the ground plane. The ITO interfaces were polymer-coated with polyimide PI-2555 and mechanically rubbed at predefined angles with respect to t to impose the director alignment and anchoring (the cases 0.5π and 0.28π are addressed in the main text). A further glass slide, parallel to plane xy (see Fig. 1), was added to seal the edge of the cell and serve as a launch window. In this way, lens-like effects and depolarization of the input beams through an NLC meniscus could be avoided. The window was covered with polyimide and rubbed at 0.25π with respect to x and y to provide a planar director alignment at the input interface. The thickness of the NLC layer (that is, across x) was $L = 100\,\mu$m, as defined by mylar spacers. The cell was filled by capillary action with an NLC E7, with refractive indices $n_{||} = 1.6954$ and $n_{\perp} = 1.5038$ at $\lambda = 1,064$ nm and Frank elastic constant $K \approx 10^{-11}$ N.

EXPERIMENTS

We injected extraordinarily polarized (fundamental order) gaussian beams of wavelength $\lambda = 1,064$ nm and waist $w \approx 3.7\,\mu$m using a $\times 20$ microscope objective. Photographic images of light evolution in the plane yz (or pt) were acquired by means of a high-resolution charge-coupled-device camera and a

microscope, collecting the light scattered by the NLC out of the plane yz. The images were filtered, digitized and colour-coded before reproduction. The beam trajectories were determined as the mean position of the transverse intensity distribution. The cells were thermally stabilized at 26 °C. All reported powers were measured in front of the sample, following the objective lens.

References

1. Stegeman, G. I. & Segev, M. Optical spatial solitons and their interactions: Universality and diversity. *Science* **286,** 1518–1523 (1999).
2. Trillo, S. & Torruellas, W. (eds) in *Spatial Solitons* (Springer, Berlin, 2001).
3. Kivshar, Y. S. & Agrawal, G. P. *Optical Solitons: From Fibers to Photonic Crystals* (Academic, New York, 2003).
4. Snyder, A. W. & Ladouceur, F. Light guiding light. *Opt. Photon. News* **10,** 35–37 (1999).
5. Kivshar, Y. S. & Stegeman, G. I. Spatial optical solitons: Guiding light for future technologies. *Opt. Photon. News* **13,** 59–63 (2002).
6. Tomlinson, W. J., Gordon, J. P., Smith, P. W. & Kaplan, A. E. Reflection of a Gaussian beam at a nonlinear interface. *Appl. Opt.* **21,** 2041–2051 (1982).
7. Aceves, A. B., Moloney, J. V. & Newell, A. C. Reflection and transmission of self-focused channels at nonlinear dielectric interfaces. *Opt. Lett.* **13,** 1002–1004 (1988).
8. Aceves, A. B., Moloney, J. V. & Newell, A. C. Theory of light-beam propagation at nonlinear interfaces. I. Equivalent-particle theory for a single interface. *Phys. Rev. A* **39,** 1809–1827 (1989).
9. Alvarado-Méndez, E. *et al.* Total internal reflection of spatial solitons at interface formed by a nonlinear saturable and a linear medium. *Opt. Commun.* **193,** 267–276 (2001).
10. Kartashov, Y., Vysloukh, V. & Torner, L. Bragg-type soliton mirror. *Opt. Express* **14,** 1576–1581 (2006).
11. Clausen, C. B. & Torner, L. Spatial switching of quadratic solitons in engineered quasi-phase-matched structures. *Opt. Lett.* **24,** 7–9 (1999).
12. Jankovic, L. *et al.* Quadratic soliton self-reflection at a quadratically nonlinear interface. *Opt. Lett.* **28,** 2103–2105 (2003).

741

13. Baronio, F., De Angelis, C., Pioger, P. H., Couderc, V. & Barthélémy, A. Reflection of quadratic solitons at the boundary of nonlinear media. *Opt. Lett.* **29**, 986–988 (2004).
14. Friedrich, L., Stegeman, G. I., Millar, P., Hamilton, C. J. & Aitchison, J. S. Dynamic, electronically controlled angle steering of spatial solitons in AlGaAs slab waveguides. *Opt. Lett.* **23**, 1438–1440 (1998).
15. Jäger, R., Gorza, S. P., Cambournac, C., Haelterman, M. & Chauvet, M. Sharp waveguide bends induced by spatial solitons. *Appl. Phys. Lett.* **88**, 061117 (2006).
16. De Gennes, P. G. & Prost, J. *The Physics of Liquid Crystals* 2nd edn (Oxford Univ. Press, London, 1993).
17. Khoo, I. C. *Liquid Crystals: Physical Properties and Nonlinear Optical Phenomena* (Wiley, New York, 1995).
18. Assanto, G., Peccianti, M. & Conti, C. Nematicons: Optical spatial solitons in nematic liquid crystals. *Opt. Photon. News* **14**, 44–48 (2003).
19. Bang, O., Krolikowski, W., Wyller, W. & Rasmussen, J. J. Collapse arrest and soliton stabilization in nonlocal nonlinear media. *Phys. Rev. E* **66**, 046619 (2002).
20. Conti, C., Peccianti, M. & Assanto, G. Observation of optical spatial solitons in a highly nonlocal medium. *Phys. Rev. Lett.* **92**, 113902 (2004).
21. Peccianti, M., Conti, C., Assanto, G., De Luca, A. & Umeton, C. Routing of anisotropic spatial solitons and modulational instability in liquid crystals. *Nature* **432**, 733–737 (2004).
22. Peccianti, M., Fratalocchi, A. & Assanto, G. Transverse dynamics of nematicons. *Opt. Express* **12**, 6524–6529 (2004).
23. Peccianti, M., Conti, C. & Assanto, G. Interplay between nonlocality and nonlinearity in nematic liquid crystals. *Opt. Lett.* **30**, 415–417 (2005).
24. Tamir, T. & Bertoni, H. L. Lateral displacement of optical beams in multilayered and periodic structures. *J. Opt. Soc. Am.* **61**, 1397–1413 (1971).
25. Emile, O., Galstyan, T., Le Floch, A. & Bretenaker, F. Measurement of the nonlinear Goos-Hänchen effect for Gaussian optical beams. *Phys. Rev. Lett.* **75**, 1511–1514 (1995).

Competing financial interests

The authors declare that they have no competing financial interests.